Available online at www.sciencedirect.com
ScienceDirect
Journal of Power Sources 161 (2006) 503–512
JOURNAL OF POWER SOURCES
www.elsevier.com/locate/jpowsour

Dynamic behaviour of methane heat exchange reformer for residential fuel cell power generation system

Keyur S. Patel, Aydin K. Sunol *

Department of Chemical Engineering, University of South Florida, 4202 E. Fowler Avenue, Tampa, FL 33620, USA

Received 25 January 2006; received in revised form 27 March 2006; accepted 28 March 2006
Available online 11 May 2006

Abstract

Due to its heat integration utility, heat exchange reformer (HER) is suitable to use for PEMFC-based residential power generation system. Since dynamics response of reformer affects overall dynamics of fuel processing system, response of HER with step change in various input parameters also needs to be studied. In this study, we present an improved distributed dynamic model for HER which is capable of computing load following characteristics. The dynamic model consists of 20 partial differential equations which are discritized using spline collocation on finite elements. Resulting differential equations along with boundary conditions are solved by stiff solver which utilizes variable order method based on numerical differentiation formulae. Step variations in various input parameters are considered and dynamic response of HER is simulated at those variations. The results provide valuable information about dynamic nature of HER which can be used to frame suitable control strategy.

Keywords: Methane heat exchange reformer; Modeling; Dynamic; Simulation

1. Introduction

In the last decade, interest in cleaner energy technologies such as fuel cells has increased significantly, particularly for power generation and automobile applications. The fuel processing system for residential power generation system based on PEMFC is explained in Fig. 1. The incoming natural gas is heated and desulphurised first. The steam is then added and methane–steam mixture is sent to the reformer. The reformate gas is cooled and passes through the first shift converter where majority of carbon monoxide is converted to carbon dioxide. The remaining carbon monoxide is removed in second shift converter. To obtain allowable levels of carbon monoxide the hydrogen rich gas is sent to PROX reactor where it is oxidized to carbon dioxide. The exit gas is sent to fuel cells to generate electricity.

The high endothermicity of the reforming reaction and limited wall heat transfer coefficients necessitate considerable energy input requirement in reformer [1]. Hence, in such circumstances, the integration of heat duties plays an important role to keep the reactor compact and, at the same time, producing the required amount of hydrogen. The methane heat exchange reformer (HER) designed by Haldor–Topsoe utilizes the concept of integrating different heat duties which results into complex flow arrangement for such reactor. Here, a combination of cocurrent and countercurrent flow arrangements between flue gas and process gas is devised to maximize the heat recovery. The HER has been used before for 250 kW Unocal MCFC demonstration project in USA and also for Dutch 50 kW MCFC system [2]. Due to its heat integration utility, such reactor can also be used to PEMFC-based residential power generation system. Another important requirement for reformer in the fuel processing system for residential power generation system is that they should operate in such a manner that it shows rapid response to the load change and also have flexible controllability. This motivates to design HER suitable for use in PEMFC-based residential power generation system and analyze its dynamic performance.

A previous simulation study on methane heat exchange reformer for MCFC power generation system simplified the model by considering each catalyst bed as a well-mixed reactor [2]. Since such simplifications do not represent the fixed bed reactors with reasonable accuracy, we present an improved dynamic model without the assumption of the well-mixed reactor suitable for use for PEMFC-based residential

* Corresponding author. Tel.: +1 813 974 3566; fax: +1 813 974 3566.
E-mail address: sunol@eng.usf.edu (A.K. Sunol).

0378-7753/$ – see front matter © 2006 Published by Elsevier B.V.
doi:10.1016/j.jpowsour.2006.03.061

Nomenclature

c_p	heat capacity (J kg^{-1} K^{-1})
c_{p_i}	heat capacity of component i (J kg^{-1} K^{-1})
C	concentration (mol m^{-3})
d	hydraulic diameter (m)
E_p	activation energy (J mol^{-1})
h	wall heat transfer coefficient (W m^{-2} K^{-1})
H_i	enthalpy of ith species (J mol^{-1})
ΔH_j	heat of reaction of jth reaction (J mol^{-1})
ΔH_{298}	heat of reaction at 298 K (J mol^{-1})
k_g	thermal conductivity of gas
k_w	thermal conductivity of wall
k_i	rate constant of reaction i
K_{e_j}	equilibrium constant of jth reaction
L	length of each catalyst bed (m)
Nu	Nusselt number (=dh/k_g)
P	partial pressure (Pa)
R	universal gas constant (J mol^{-1} K^{-1})
Re	Reynolds number (=$du\rho_g/k_g$)
$R_{r,i}$	rate of reaction i (mol s^{-1} kg^{-1} catalyst)
$r_{r,i}$	rate of generation of component i in reformer (mol s^{-1} kg^{-1} catalyst)
S_r	heat transfer area per unit volume (m^2/m^3)
t	time (s)
t_w	thickness of wall (m)
T	temperature (K)
T_{ref}	reference temperature (298 K)
u	superficial velocity (m s^{-1})
z	length of reactor (m)

Greek symbol

ρ	density (kg m^{-3})

Subscripts

g	gas
i	ith reactant
j	jth reaction
f	flue gas
f1	first flue gas channel
f2	second flue gas channel
p1	process gas channel
p2	product gas channel
r	catalyst bed
r1	first catalyst bed
r2	second catalyst bed
w	wall
w1	first wall
w2	second wall
w3	third wall
w4	fourth wall

power generation system. The model consists of 12 partial differential equations which are descritized using orthogonal spline collocation on finite elements. The resulting ordinary differential equations along with boundary conditions are solved numerically and dynamic performance of HER for step variations in various input parameters is simulated.

2. Reactor geometry

As shown in Fig. 2 [3], the Haldor–Topsoe HER comprises of pressure vessel, two catalyst bed and burner. The reformer fuel is combusted in the burner located at the bottom of the pressure vessel. Feed gas flows downwards through first catalyst bed where it is heated by convection from both the flue gas and the reformed product gas, both flowing countercurrent to the feed. After leaving the first catalyst bed, the partially reformed gas is fed to the top of second catalyst bed where it is heated by flue gas and the partially reformed process gas as shown in Fig. 2. Both catalyst beds are filled with Ni/MgO–Al_2O_3 catalyst where steam reforming of methane takes place. It is also clear from Fig. 1 that the section of the reactor to the left of the burner channel consists of six channels including two channels for fixed bed reactor, two channels for the process gas and the outer two channels for the flue gas flow. Each channel of the reactor is considered to have rectangular cross section. Due to symmetry of the reactor, only one section of the reactor is modeled.

3. Reaction-scheme and kinetics

3.1. Reformer

Steam reforming of methane takes place in presence of the Ni/MgO–Al_2O_3 catalyst which is described by following reaction.

$$CH_4 + H_2O \leftrightarrow CO + 3H_2, \quad \Delta H_{298} = 206\,\text{kJ mol}^{-1} \tag{1}$$

$$CO + H_2O \leftrightarrow CO_2 + H_2, \quad \Delta H_{298} = -41\,\text{kJ mol}^{-1} \tag{2}$$

$$CH_4 + 2H_2O \leftrightarrow CO_2 + 4H_2, \quad \Delta H_{298} = 165\text{kJ mol}^{-1} \tag{3}$$

Kinetic information for these reactions is taken from Xu and Froment [4].

$$R_{r,1} = \frac{k_2}{P_{H_2}^{2.5}} \left(P_{CH_4} P_{H_2O} - \frac{P_{H_2}^3 P_{CO}}{K_{e_1}} \right) \frac{1}{Q_r^2} \tag{4}$$

$$R_{r,2} = \frac{k_3}{P_{H_2}} \left(P_{CO} P_{H_2O} - \frac{P_{H_2} P_{CO_2}}{K_{e_2}} \right) \frac{1}{Q_r^2} \tag{5}$$

$$R_{r,3} = \frac{k_4}{P_{H_2}^{3.5}} \left(P_{CH_4} P_{H_2O}^2 - \frac{P_{H_2}^4 P_{CO_2}}{K_{e_3}} \right) \frac{1}{Q_r^2} \tag{6}$$

where

$$Q_r = 1 + K_{CO} P_{CO} + K_{H_2} P_{H_2} + K_{CH_4} P_{CH_4} + \frac{K_{H_2O} P_{H_2O}}{P_{H_2}}$$

3.2. Burner

Reaction scheme for the burner is as below

$$CH_4 + 2O_2 \leftrightarrow CO_2 + 2H_2O, \quad \Delta H_{298} = -802.3\,\text{kJ mol}^{-1} \tag{7}$$

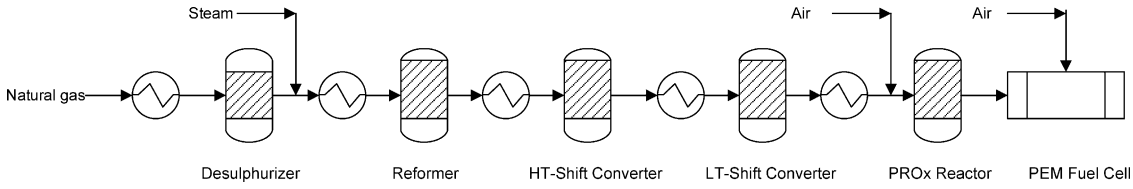

Fig. 1. Fuel processing system.

$$0.5O_2 + H_2 \leftrightarrow H_2O, \quad \Delta H_{298} = -241.8\,\text{kJ mol}^{-1} \tag{8}$$

$$CO + 0.5O_2 \leftrightarrow CO_2, \quad \Delta H_{298} = -283\,\text{kJ mol}^{-1} \tag{9}$$

The rate equations for catalytic combustion are not included in the model equations. Assuming that combustion reactions are comparatively faster than stem reforming reaction, flue gas temperature and composition at burner outlet can be obtained from equilibrium calculations.

4. Simulation model

Both fixed bed catalyst beds are modeled as one-dimensional pseudo-homogenous reactor of the equal length and of equal catalyst bed density. In order to simplify the model, following assumptions are made:

- Pressure inside both the flue gas and the reformer channels is assumed to be constant.
- Conduction and convection are assumed to be predominant heat transfer mechanism while radiation effect is neglected.
- Heat loss to surroundings is neglected.
- Both the process gas and the fuel gas are treated as ideal gas.

4.1. Mass balance equations

Based on these assumptions stated before, mass balance equations can be expressed as partial differential equations as follows:

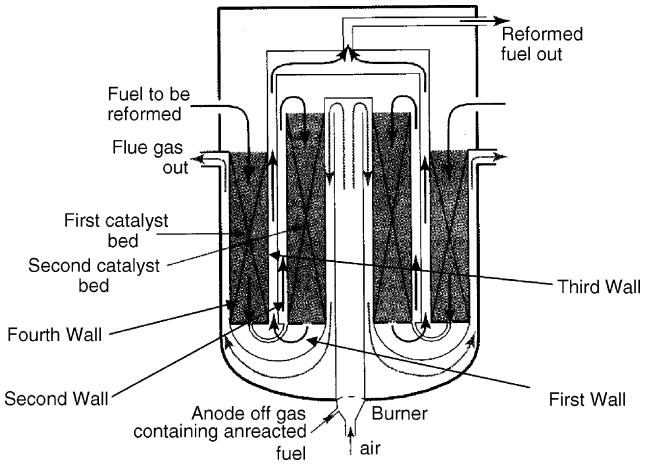

Fig. 2. Schematic diagram of the reactor [3].

- First catalyst bed:

$$\frac{\partial C_{r1,i}}{\partial t} = -u_r \frac{\partial C_{r1,i}}{\partial z} + \rho_r r_{r1,i}, \quad i = 1\text{–}5 \tag{10}$$

- Second catalyst bed:

$$\frac{\partial C_{r2,i}}{\partial t} = -u_r \frac{\partial C_{r2,i}}{\partial z} + \rho_r r_{r2,i}, \quad i = 1\text{–}5 \tag{11}$$

4.2. Energy balance equations

Similarly, energy balance equations are given by partial differential equations. Here, the first and the second wall refer to the two opposite sides of the second catalyst bed along which the gas flow occurs. Similarly, the third and the fourth wall form the opposite sides of the second catalyst bed. The first flue gas channel and the first process gas channel are on the opposite sides of the second catalyst bed while the second flue gas channel and the second preheat channel are on the opposite sides of the first catalyst bed as shown in Fig. 3. With this introduction of the nomenclature, the energy balance equations can be written as follows:

- First catalyst bed:

$$\rho_r c_{p_{r1}} \frac{\partial T_{r1}}{\partial t} = -u\rho_r c_{p_{r1}} \frac{\partial T_{r1}}{\partial z} + \rho_r \sum_{j=1}^{3} R_{r1,j}(-\Delta H_{r1,j}) + h_{r1} S_{r1}(T_{w4} - T_{r1}) + h_{r1} S_{r1}(T_{w3} - T_{r1}) \tag{12}$$

- Second catalyst bed:

$$\rho_r c_{p_{r2}} \frac{\partial T_{r2}}{\partial t} = -u\rho_r c_{p_{r2}} \frac{\partial T_{r2}}{\partial z} + \rho_r \sum_{j=1}^{3} R_{r2,j}(-\Delta H_{r2,j}) + h_{r2} S_{r2}(T_{w1} - T_{r2}) + h_{r2} S_{r2}(T_{w2} - T_{r2}) \tag{13}$$

- Flue gas channel 1:

$$\rho_f c_{p_f} \frac{\partial T_{f1}}{\partial t} = -u_f \rho_f c_{p_f} \frac{\partial T_{f1}}{\partial z} + h_{f1} S_{f1}(T_{w1} - T_{f1}) \tag{14}$$

- Flue gas channel 2:

$$\rho_f c_{p_f} \frac{\partial T_{f2}}{\partial t} = -u_f \rho_f c_{p_f} \frac{\partial T_{f2}}{\partial z} + h_{f2} S_{f2}(T_{w4} - T_{f2}) \tag{15}$$

- Process gas channel:

$$\rho_{p1} c_{p_{p1}} \frac{\partial T_{p1}}{\partial t} = -u_r \rho_{p1} c_{p_{p1}} \frac{\partial T_{p1}}{\partial z} + h_{p1} S_{p1}(T_{w2} - T_{p1}) \tag{16}$$

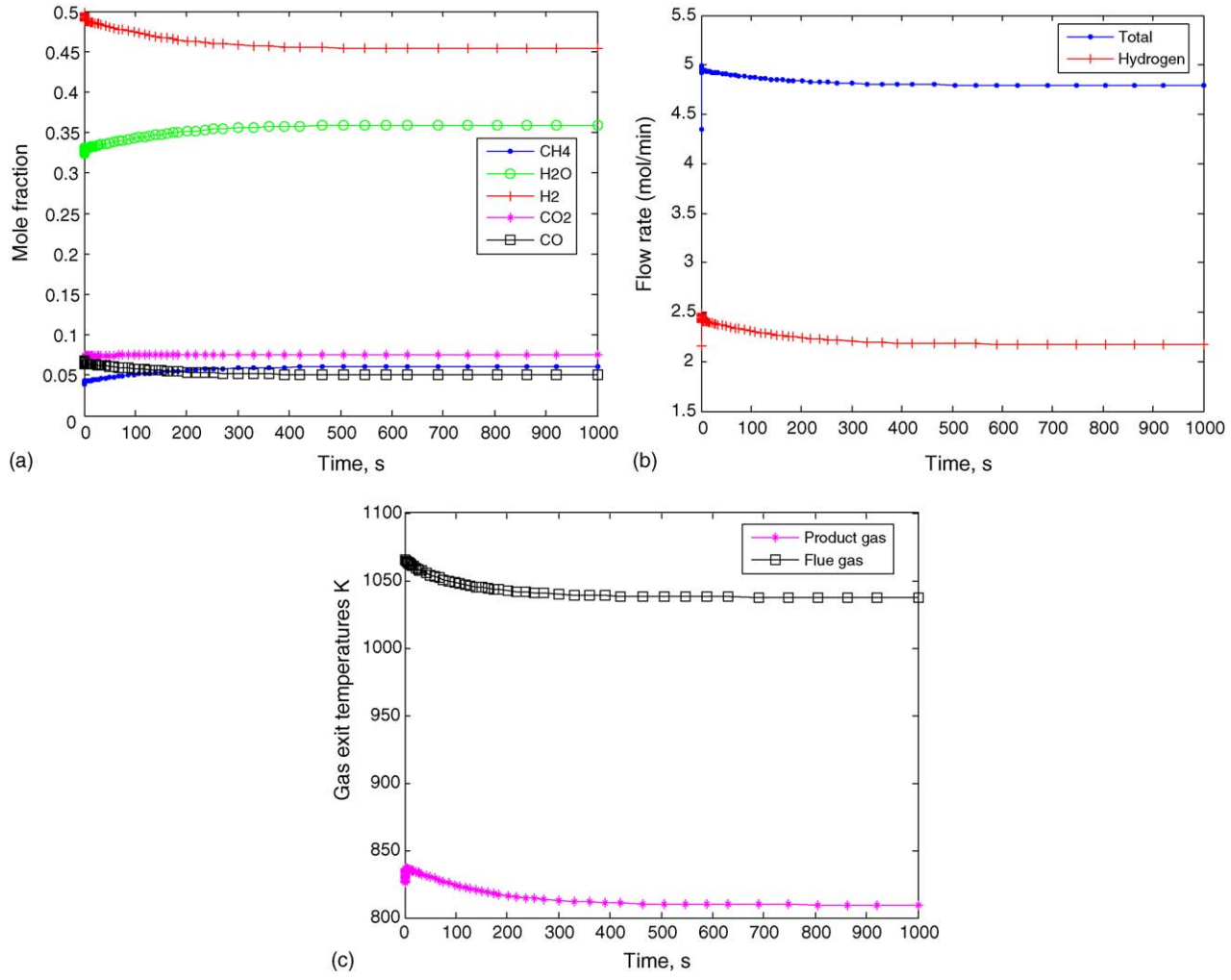

Fig. 3. Dynamic behavior of HER for 15% step increase in inlet process gas flow: (a) product gas composition, (b) product gas flow rate and (c) exit gas temperatures.

- Product gas channel:

$$\rho_{p2}c_{p_{p2}}\frac{\partial T_{p2}}{\partial t} = -u_r\rho_{p2}c_{p_{p2}}\frac{\partial T_{p2}}{\partial z} + h_{p2}S_{p2}(T_{w3} - T_{p2}) \tag{17}$$

- First wall:

$$\rho_w c_{p_w}\frac{\partial T_{w1}}{\partial t} = k_w\frac{\partial^2 T_{w1}}{\partial z^2} + \frac{h_{f1}}{t_w}(T_{f1} - T_{w1}) + \frac{h_{r1}}{t_w}(T_{r1} - T_{w1}) \tag{18}$$

- Second wall:

$$\rho_w c_{p_w}\frac{\partial T_{w2}}{\partial t} = k_w\frac{\partial^2 T_{w2}}{\partial z^2} + \frac{h_{p1}}{t_w}(T_{p1} - T_{w2}) + \frac{h_{r1}}{t_w}(T_{r1} - T_{w2}) \tag{19}$$

- Third wall:

$$\rho_w c_{p_w}\frac{\partial T_{w3}}{\partial t} = k_w\frac{\partial^2 T_{w3}}{\partial z^2} + \frac{h_{p2}}{t_w}(T_{p2} - T_{w3}) + \frac{h_{r2}}{t_w}(T_{r2} - T_{w3}) \tag{20}$$

- Fourth wall:

$$\rho_w c_{p_w}\frac{\partial T_{w4}}{\partial t} = k_w\frac{\partial^2 T_{w4}}{\partial z^2} + \frac{h_{f2}}{t_w}(T_{f2} - T_{w4}) + \frac{h_{r1}}{t_w}(T_{r1} - T_{w4}) \tag{21}$$

The following boundary conditions are added to the modeling equations.

Here, the top of each channel and each catalyst bed is considered as $z = 0$ and the bottom as $z = L$.

At $z = 0$

$$\frac{\partial T_{w1}(t)}{\partial z} = \frac{\partial T_{w2}(t)}{\partial z} = \frac{\partial T_{w3}(t)}{\partial z} = \frac{\partial T_{w4}(t)}{\partial z} = 0 \tag{22}$$

$$C_{r1,i}(t) = C_{r1,i}(0), \quad i = 1\text{–}5 \tag{23}$$

$$C_{r2,i}(t)|_{z=0} = C_{r1,i}(t)|_{z=L}, \quad i = 1\text{–}5 \tag{24}$$

$$T_{r1}(t) = T_{r1}(0) \tag{25}$$

$$T_{r2}(t)|_{z=0} = T_{p1}(t)|_{z=L} \tag{26}$$

Boundary conditions at $z = L$

$$\frac{\partial T_{w1}(t)}{\partial z} = \frac{\partial T_{w2}(t)}{\partial z} = \frac{\partial T_{w3}(t)}{\partial z} = \frac{\partial T_{w4}(t)}{\partial z} = 0 \quad (27)$$

$$T_{r2}(t)|_{z=L} = T_{p2}(t)|_{z=L} \quad (28)$$

4.3. Heat transfer coefficients

The reformer wall heat transfer coefficient is estimated from correlation (29) [5].

$$Nu = 0.027 C_C (Re)^{0.8} (Pr)^{0.33} \quad (29)$$

where C_C is constant which depends on size of the catalyst particles.

Depending on the type of the flue gas flow, the heat transfer coefficient can be estimated from following correlations [6].

For laminar flow of the flue gas:

$$Nu = 1.86 \left(RePr \frac{d}{L} \right)^{1/3} \quad (30)$$

For turbulent flow of the flue gas:

$$Nu = 0.027 (Re)^{0.8} (Pr)^{0.33} \quad (31)$$

4.4. Fluid, catalyst and wall properties

Thermal conductivity of fuel gas can be expressed as a function of temperature from (32) [7].

$$k_g = 1.679 \times 10^{-2} + 5.073 \times 10^{-5} T \quad (32)$$

Enthalpy of component i in reformer gas is given by (33):

$$H_i = \int_{T_{ref}}^{T} c_{p_i} \, dT \quad (33)$$

Heat capacity of gas species is evaluated as a function of temperature from (34):

$$c_{p_i} = a + bT + cT^2 \quad (34)$$

Viscosity of reformer gas mixture is evaluated as function of concentration and temperature using corresponding states methods [8].

Thermal conductivities and heat capacities of reformer catalyst is taken as that of alumina [6]. Thermal conductivity and heat capacity of wall is taken as that of iron [6]. Thermal conductivities of individual gas species is taken from [9]. From component thermal conductivity, mixture thermal conductivity can be estimated using method of Linsay and Bromley [10].

4.5. Numerical technique

The set of 20 partial differential equations ((10)–(21)) are discritized using orthogonal spline collocation on finite elements [11]. The reactor length is divided into 10 intervals with two collocation points in each interval. Discritized partial differential equations along with boundary conditions form system of stiff differential algebraic equations which are solved using stiff integrator that utilizes variable order solver based on numerical differentiation formulae. The computations are performed in MATLAB programming environment.

5. Results and discussion

The base case reformer configuration is shown in Table 1. Simulation results for this configuration shows that HER generates 4.32 mol min^{-1} of hydrogen flow which corresponds to 6.96 kW power assuming 40% efficiency for fuel cell system. This is taken as reference state and following step variations are considered to study dynamic performance of HER:

- ±15% step changes in inlet process gas flow rate;
- ±15% step changes in process gas pressure;
- ±15% step changes in inlet burner flue gas pressure and flue gas flow rate;
- ±15% step changes in steam to methane ratio;
- step change in process gas inlet temperature from 400 to 460 K.

5.1. Dynamics of process gas flow rate

The residential fuel cell power system is often required to operate under partial load. To enable to get different power output, manipulation of inlet process gas flow of the reformer can be one of the possible variations. Hence, dynamic performance of the HER under ±15% step variations in inlet process gas flow is analyzed here.

Simulated composition profiles of the product gas for step increase in process gas flow rate are shown in Fig. 3(a). Results indicate that methane and steam compositions increase while hydrogen composition decreases with time. This trend is similar to the experimentally observed dynamic concentration profile [12]. The hydrogen composition decreases from 49.72% to 45.35% with net gain of −4.37%. Similarly, methane concentration increases from 3.85% to 6.11% with net gain of 2.26%. For step decrease in process gas flow rate, it is found that methane composition decreases from 3.85% to 1.74% with net gain of −2.11% while hydrogen composition increases from 49.72% to 53.3% with net gain of 3.58%. Results show that all responses

Table 1
Design specifications and operating conditions for the base case

Design specification/operating condition	Value
Length of each catalyst bed	1 m
Reformer channel thickness	0.01 m
Thickness of each flue gas channel thickness	0.01 m
Thickness of each preheat channel thickness	0.01 m
Reformer catalyst bed density	100 kg m^{-3}
Wall thickness	1×10^{-3} m
Reformer pressure	2 bar
Burner pressure	8 bar
Steam/methane ratio	3
Reformer inlet gas temperature	400 K
Reformer inlet gas flow	0.1083 mol s^{-1}
Flue gas flow	0.6873 mol s^{-1}

are stable without any overshoot and reaches stead state within 500 s.

For step increase in process gas flow rate, the total molar flow rate increases from 4.34 to 4.79 mol min^{-1} with net gain of 10.36% and hydrogen flow rate increases from 2.16 to 2.174 mol min^{-1} with net gain of 0.648% as shown in Fig. 3(b). Similarly, the step decrease in flow rate decreases in total molar flow rate to 3.838 mol min^{-1} and hydrogen flow rate to 2.046 mol min^{-1} with net gains of −11.65% and −5.28%, respectively. Also, its should be noted that for both cases, flow rates increases rapidly, reaches maximum and then decreases with slight overshoot. This dynamic behavior of HER matches in quality with the previous simulation studies [2]. Higher gain in total molar flow rate suggests that the step change in inlet flow rate is suitable strategy for manipulating total flow rate of product gas.

Fig. 3(c) shows thermal behavior of HER. For step increase in flow rate, product gas temperature increases initially from 826 to 836.6 K and then decreases to steady state value of 806.9 K with net gain of −2.31%. Flue gas temperature decreases from 1066 to 1038 K with net gain of −2.63%. Similarly, on step decrease in process gas flow, the process gas temperature first decreases to 813.6 K and then increases to 845.7 K with net gain of 2.39%. Flue gas temperature increases to 1098 K with net gain of 3%. Although, all the temperature responses reach steady state within 500 s, overshoots in thermal response can affect overall performance of fuel processing system.

5.2. Dynamics of process gas pressure

Pressure change is one of the important parameters that can affect desirable operation of HER. Therefore, dynamic performance of HER with ±15% step increase/decrease of pressure is analyzed in this section.

As shown in Fig. 4(a), 15% step decrease in process gas pressure decreases methane molar composition from 3.85% to 1.49% with net gain of −2.36% while hydrogen composition increases from 49.72% to 53.8% with net gain of 4.08%. Similarly, for step increase in process gas pressure, methane concentration is found to increase from 3.85% to 6.33% with net gain of 2.48% and hydrogen composition decreases from 49.72% to 44.85% with net gain of −4.87%. Results show that all responses are stable without any overshoot and reaches stead state within 500 s.

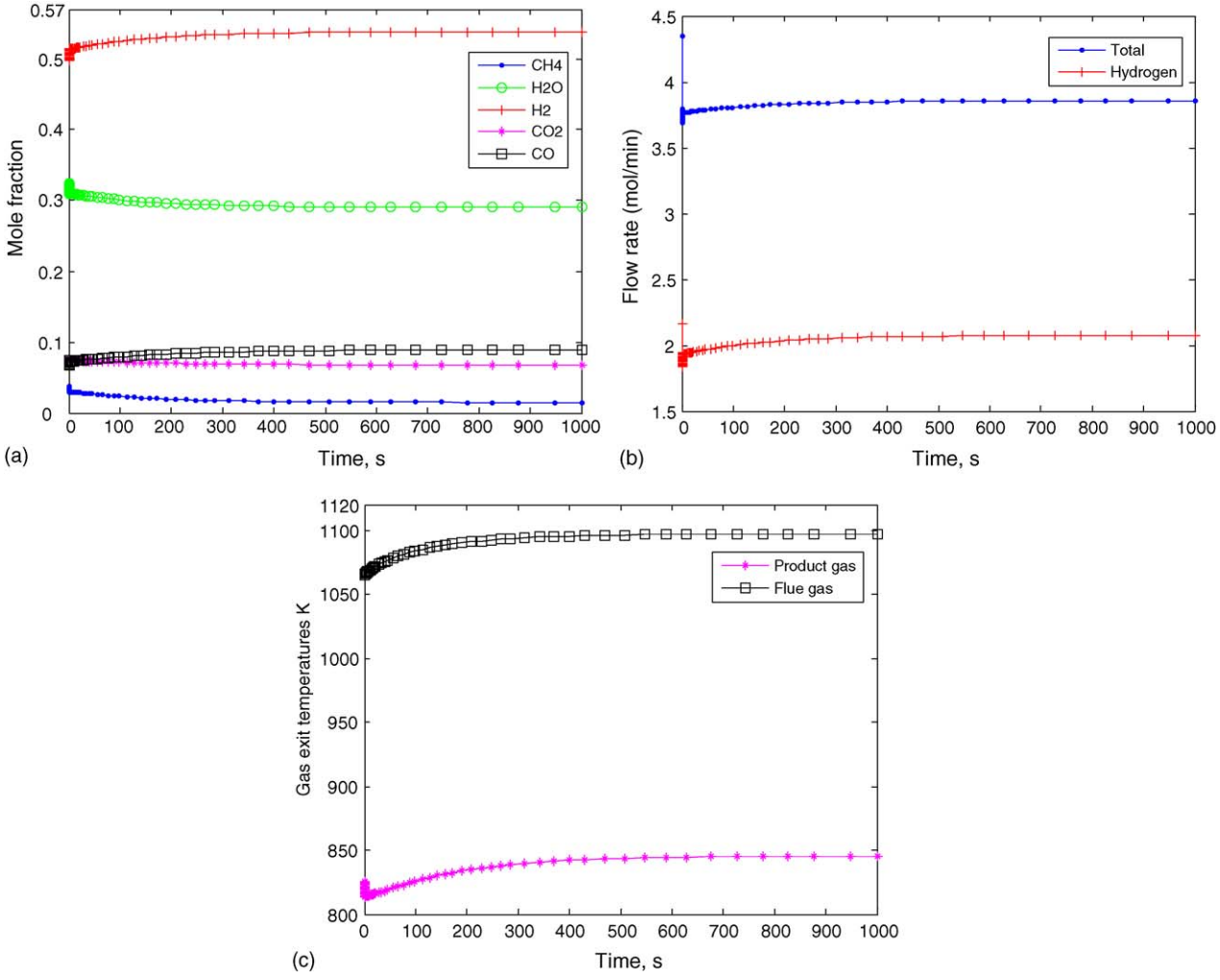

Fig. 4. Dynamic behavior of HER for 15% step decrease in process gas pressure: (a) product gas composition, (b) product gas flow rate and (c) exit gas temperatures.

For step decrease in process gas pressure, the total molar flow rate decreases from 4.34 to 3.86 mol min^{-1} with net gain of −11.06% and hydrogen flow rate decreases from 2.16 to 2.076 mol min^{-1} with net gain of −3.89% as shown in Fig. 4(b). Similarly, the step increase in process gas pressure causes increase in total molar flow rate to 4.78 mol min^{-1} with net gain of 10.14%. The hydrogen flow rate decreases to 2.14 mol min^{-1} with net gain of −0.93%. Also, is should be noted that for both cases, flow rates changes rapidly, reaches extreme value and then approaches the steady state value with slight overshoot.

Fig. 4(c) shows thermal behavior of HER. For step decrease in process gas pressure, product gas temperature decreases initially from 826 to 813.6 K and then increases to steady state value of 845.5 K with net gain of 2.39%. Flue gas temperature increases from 1066 to 1098 K with net gain of 3%. Similarly, on step increase in process gas pressure, the process gas temperature first increases to 836.4 K and then decreases to 810.6 K with net gain of −1.86%. Flue gas temperature decreases to 1038 K with net gain of −2.63%. It is found that all the temperature responses reach steady state within 500 s.

5.3. Dynamics of inlet process gas temperature

Since inlet process gas is heated and partially reformed in first bed in HER, inlet temperature plays important role in overall performance of HER. Hence, dynamics of step increase of inlet process gas temperature from 400 to 460 K is studies in this section.

As shown in Fig. 5(a), product gas composition dynamics with step increase in process gas temperature is faster that earlier discussed variations. Hydrogen concentration increases from 49.72% to 55.54% and then approaches to steady state value of 51.07% with net gain of 1.35%. Similarly, methane concentration decreases from 3.85% to 0.269% and approaches steady state value of 3.11% with net gain of −0.74%. Results also reveal that the composition response is faster and reaches steady state in about 10 s.

Fig. 5(b) explains the flow rate variations. The total molar flow rate decreases from 4.34 to 3.78 mol min^{-1}, increases to 4.365 mol min^{-1} and then decreases to 3.82 mol min^{-1} with net gain of −11.98%. Hydrogen molar flow rate shows similar behavior. It decreases from 2.16 to 1.88 mol min^{-1}, increases

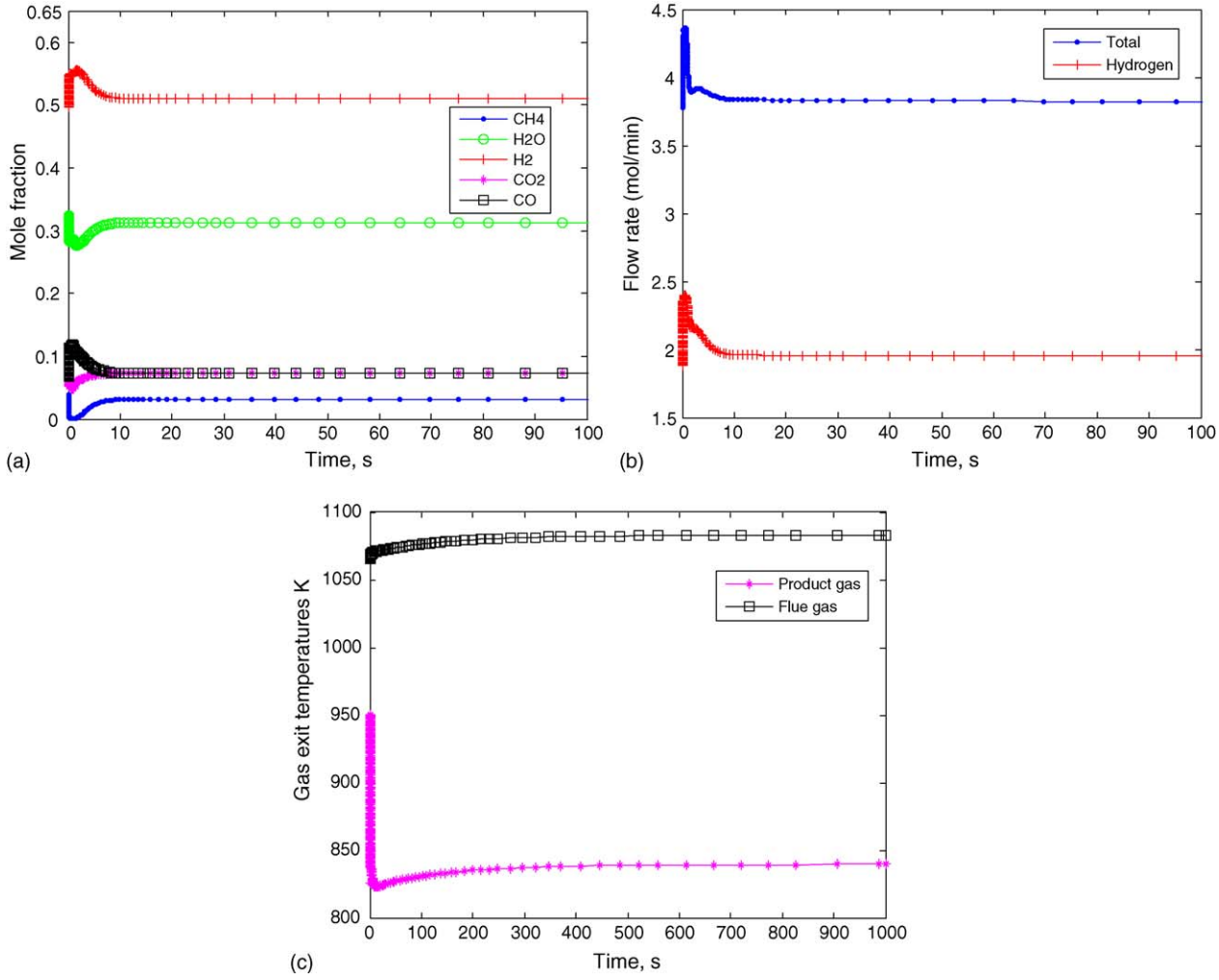

Fig. 5. Dynamic behavior of HER for step increase in process gas temperature from 400 to 460 K: (a) product gas composition, (b) product gas flow rate and (c) exit gas temperatures.

to 2.4 mol min^{-1} and then decreases to 1.95 mol min^{-1} with net gain of −9.72%. Also, is should be noted that for both cases, flow rates changes rapidly, with the steady state value reaches only in about 10 s.

As shown in Fig. 5(c), product gas temperature increases initially from 826 to 950 K and then decreases to steady state value of 839 K with net gain of 1.57%. Flue gas temperature decreases from 1066 to 1083 K with net gain of 1.59%. It is found that thermal response of HER is slower than flow response and reaches steady state values in about 500 s.

5.4. Dynamics of flue gas pressure and flue gas flow rate

Since steam reforming is highly endothermic reaction, flue gas pressure plays important role to maintain high temperature and thus creates favorable condition for steam reforming. Here, dynamic performance of HER for step variation of flue gas pressure is analyzed.

As shown in Fig. 6(a), step increase in flue gas pressure decreases methane composition from 3.85% to 2.32% with net gain of −1.53% and increases hydrogen composition from 49.72% to 52.3% with net gain of 2.58%. Similarly for step decrease in burner pressure, net gains in methane and hydrogen compositions are found to be −4.01% and 2.13%. Results reveal that all responses are stable without any overshoot and reaches stead state within 500 s.

For step increase, the total molar flow rate increases from 4.34to 4.46 mol min^{-1} with net gain of 2.77% and hydrogen flow rate increases from 2.16 to 2.33 mol min^{-1} with net gain of 7.87% as shown in Fig. 6(b). Same way, the step decrease in burner pressure causes net gain of −3.45% and −11.3% in total and hydrogen molar flow rate, respectively. Responses indicated that steady state is reached in about 500 s. The gain values also suggest that fluctuation in burner inlet pressure effects hydrogen molar flow rate more than the total molar flow rate.

Fig. 6(c) shows thermal behavior of system. For step increase in flue gas pressure, product gas temperature increases from 826 to 852 K with net gain of 3.15%. Flue gas temperature increases from 1066 to 1098 K with net gain of 3%. Similarly, step decrease in burner pressure causes decrease in product gas temperature and flue gas temperature with net gains of −3.63%

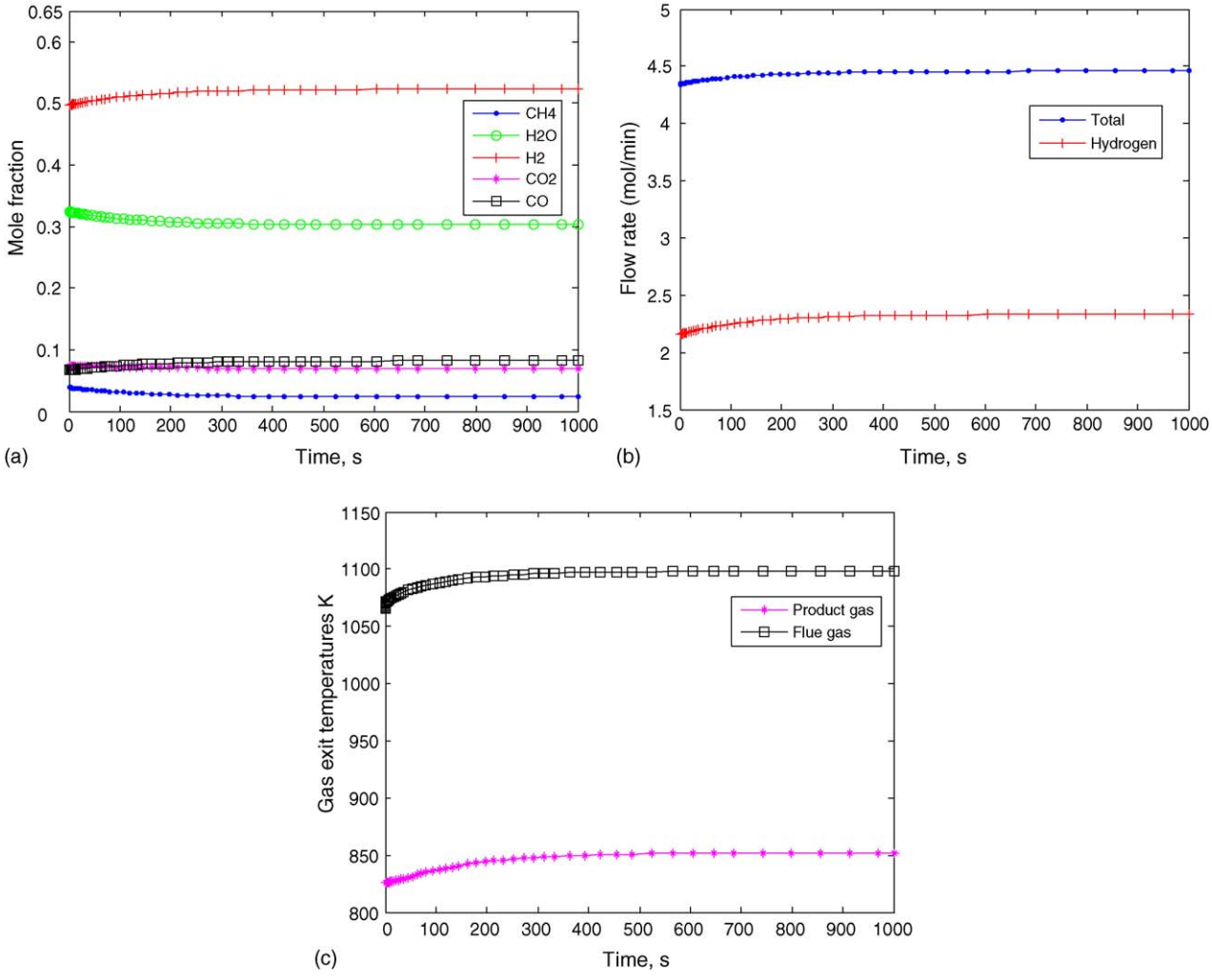

Fig. 6. Dynamic behavior of HER for 15% step increase in flue gas pressure: (a) product gas composition, (b) product gas flow rate and (c) exit gas temperatures.

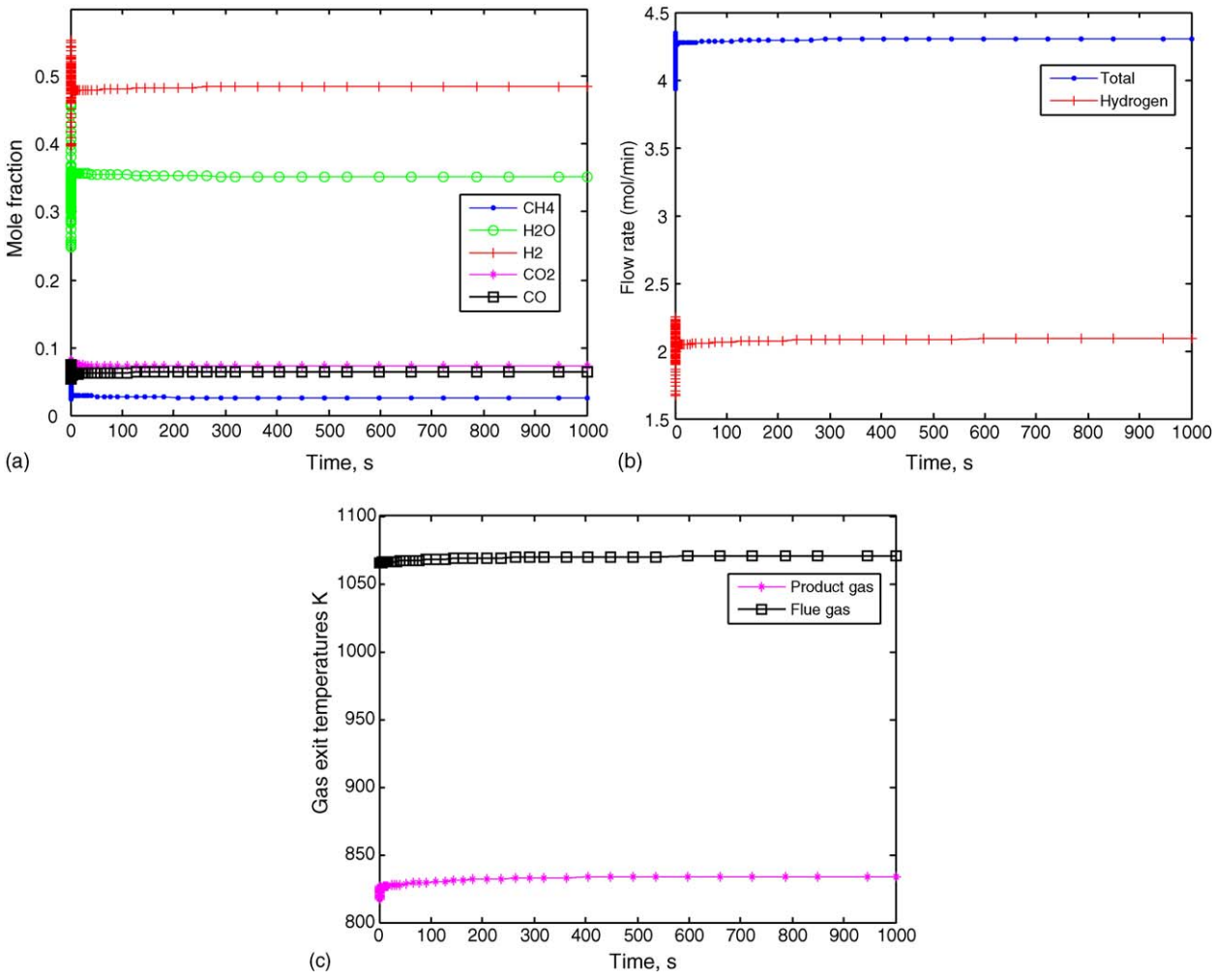

Fig. 7. Dynamic behavior of HER for 15% step increase in steam to methane ratio: (a) product gas composition, (b) product gas flow rate and (c) exit gas temperatures.

and −3.66%, respectively. All the temperature responses reach steady state within 500 s without any overshoot. Simulated results for step variation in flue gas flow rate show similar gains for compositions, flow rates and temperatures.

5.5. Dynamics of steam to methane ratio

Dynamic performance of HER with step increase/decrease of steam to methane ratio is analyzed in this section.

For 15% step increase in steam to methane ratio, overshoots are observed in compositions of all components as shown in Fig. 7(a). Hydrogen composition decreases from 49.72% to 48.51% with net gain of −1.21%. Methane composition also decreases from 3.85% to 2.54% with net gain of −1.31%. It is observed that the response is fast and reaches steady state value in just 5 s. Similarly, for 15% step decrease in steam to methane ratio, hydrogen and methane compositions are found to increase to 50.64% and 5.65%, respectively.

As with compositions, overshoots are also observed in total molar flow rate and hydrogen molar flow rate as shown in Fig. 7(b). Total flow rate decreases from 4.34 to 4.303 mol min^{-1} with net gain of −0.85% and hydrogen molar flow rate decreases from 2.16 to 2.088 mol min^{-1} with net gain of −3.33%. It is found that both the responses are fast with major response achieved only in 5 s. For step decrease in stem to methane ratio, total flow rate increases from 4.34 to 4.38 mol min^{-1} with net gain of 0.69% and hydrogen flow rate increases from 2.16 to 2.22 mol min^{-1} with net increase of 2.6%.

As shown in Fig. 7(c), step increase in steam to methane ratio causes increase in product from 826 to 834 K with net gain of 0.97% and increase in flue gas temperature from 1066 to 1070 K with net gain of 0.38%. For step decrease in steam to methane ratio, product gas temperature is found to decrease to 818.3 K with gain of −0.93% and flue gas temperature also decreases to 1061 K with gain of −0.47%.

6. Conclusion

In this work, we numerically investigated dynamic performance of methane heat exchange reformer that is suitable to be used for PEMFC-based residential power generation system. Improved distributed model for HER is presented and dynamic effects of step variations in various input variables are simulated. Model equations form coupled partial differen-

tial equations which are descritized using spline collocation on finite elements and solved numerically. The simulation results indicate higher gains in total molar flow rate by step changes in process gas flow rate and process gas pressure with slight overshoot. Product gas temperature shows overshoot for step changes in flow rate or pressure of process gas. Higher gains in hydrogen flow rate and comparatively lower gains in total molar flow rate are obtained with variations in flue gas velocity or flue gas pressure. Furthermore, product gas temperature does not show any overshoot for step changes in flue gas pressure or flue gas velocity. Response time for steady states is found to be 500 s for all these variations. Step changes in inlet process gas temperature show rapid (steady state value reaches in 10 s) response and higher gains in total and hydrogen flow rates with overshoots. The product gas temperature for this variation shows overshoot and reaches steady state in 500 s. Flow rates show overshoots for step variation in steam to methane ratio. Also, product gas temperature and total flow rate are found to be less sensitive to variations in steam to methane ratio.

References

[1] J.R. Rostrup-Nielsen, in: J.R. Anderson, M. Boudart (Eds.), Catalysis, Science and Technology, Catalytic Steam Reforming, vol. 5, Springer, Berlin, 1984.
[2] W. He, Fuel Process. Technol. 53 (1997) 99–113.
[3] L. James, A. Dicks, Fuel Cell Systems Explained, 2nd ed., Wiley, 2003, p. 257.
[4] J. Xu, G.F. Froment, AIChE J. 35 (1) (1989) 88–96.
[5] E.L. Cussler, Diffusion, Mass Transfer in Fluid Systems, Cambridge University Press, Cambridge, 1984.
[6] R.H. Perry, D.W. Green, Perry's Chemical Engineers' Handbook, 7th ed., McGraw-Hill, New York, 1997, pp. 2-334–2-337.
[7] F.P. Incropera, D.P. DeWitt, Introduction to Heat Transfer, Wiley, New York, 1990.
[8] K. Lucas, Phase Equilibria and Fluid Properties in the Chemical Industry, Dechema, Frankfurt, 1980.
[9] Y.A. Cengel, R.H. Turner, Fundamentals of Thermal Fluid Science, McGraw-Hill, New York, 2001.
[10] A.L. Linsay, L.A. Bromley, Ind. Eng. Chem. 42 (1950) 1508.
[11] C.D. Boor, A Practical Guide to Splines, Springer-Verlag, New York, 1978, pp. 277–298.
[12] H.J. Jahn, W. Schroer, J. Power Sources 150 (2005) 101–109.